

# Collisional properties of trapped cold chromium atoms

Zoran Pavlović<sup>1</sup>, Björn O. Roos<sup>2</sup>, Robin Côté<sup>1</sup>, and H. R. Sadeghpour<sup>3</sup>

<sup>1</sup>*Physics Department, University of Connecticut, 2152 Hillside Rd., Storrs, CT 06269-3046*

<sup>2</sup>*Department of Theoretical Chemistry, Chemical Center, P.O.B. 124 S-221 00 Lund, Sweden and*

<sup>3</sup>*ITAMP, Harvard-Smithsonian Center for Astrophysics, 60 Garden Street, Cambridge, MA 02138.*

(Dated: February 12, 2018)

We report on calculations of the elastic cross section and thermalization rate for collision between two maximally spin-polarized chromium atoms in the cold and ultracold regimes, relevant to buffer-gas and magneto-optical cooling of chromium atoms. We calculate *ab initio* potential energy curves for Cr<sub>2</sub> and the van der Waals coefficient  $C_6$ , and construct interaction potentials between two colliding Cr atoms. We explore the effect of shape resonances on elastic cross section, and find that they dramatically affect the thermalization rate. Our calculated value for the *s*-wave scattering length is compared in magnitude with a recent measurement at ultracold temperatures.

Collisions of atoms at ultracold temperatures have received considerable attention because of their importance in cooling and trapping of atoms [1] and their role in high precision spectroscopy [2] and Bose-Einstein condensation [3]. Processes occurring in the cold regime are sensitive to the details of the interaction potentials between the colliding systems over an extended range of inter-nuclear separations. Recent experiments with chromium [4, 5, 6, 7] emphasize the need for theoretical studies of Cr scattering properties. The interest in cooling Cr stems from its particular properties; in its ground state  $^7S_3$ , it possesses a very large magnetic moment,  $6 \mu_B$  ( $\mu_B$ : Bohr magneton), making it an ideal atom for buffer-cooling in a purely magnetic trap [7], as well as for magneto-optical trapping [4]. In addition, anisotropic long-range interactions, such as chromium's magnetic dipole-dipole interactions, may lead to novel phenomena in BECs [9, 10]. The existence of a stable fermionic isotope,  $^{53}\text{Cr}$ , opens the possibility of obtaining fermionic degenerate gas using sympathetic cooling. Chromium was also used in a new cooling scheme [5], where ultracold chromium atoms were loaded from a MOT into an Ioffe-Pritchard magnetic trap, and cooled below  $100\mu\text{K}$ . However, a not so-desirable byproduct of large-spin collision is inelastic “bad” scattering rates that deplete the trap.

On the theoretical front, the electronic spectrum of the Cr<sub>2</sub> dimer poses a considerable numerical challenge. Chromium is the first atom in the periodic table with a half-filled *d* shell (the ground electronic configuration is Cr( $3d^5 4s, ^7S$ )) and the Cr<sub>2</sub> dimer is one of the most extreme cases of multiple metal-metal bonding. To date, the best attempt to calculate its interaction potential curves is a multiconfiguration second-order perturbation theory with complete active space self-consistent field (CASSCF/CASPT2) [11, 12]. While some information on the spectroscopy of the ground electronic state ( $^1\Sigma_g^+$  molecular symmetry) exists, there is no data available for the interaction of two maximally spin-stretched Cr atoms in the  $^{13}\Sigma_g^+$  molecular symmetry, i.e. total spin,  $S = 6$ .

In this communication, we explore the collisional properties of Cr atoms in the cold and ultracold temperature regimes by revisiting the electronic structure of the dimer. More accurate Born-Oppenheimer potential en-

ergy curves dissociating to two ground Cr atoms were obtained. The van der Waals interaction coefficient,  $C_6$ , was obtained semi-empirically from available bound atomic transition matrix elements and photoionization cross sections to be  $C_6 = 745 \pm 55$  a.u., where 1 a.u. =  $9.57 \times 10^{-80}$  Jm<sup>6</sup>. The elastic cross section and collision rate coefficient were calculated using the newly constructed potential curves and compared against two recent measurements of elastic rate coefficients [5, 7]. We also investigated the bound and resonance structure in the  $^{13}\Sigma_g^+$  potential energy curve and determined the resonance positions and widths as a function of rotational angular momenta.

The potential curves for Cr<sub>2</sub>, shown in Fig. 1, were constructed from three regions joined smoothly together. We first computed *ab initio* potential curves using the CASSCF/CASPT2 method [11, 12]. The CASSCF wave function is formed by distributing 12 electrons in the 3d and 4s derived active orbitals while keeping the inactive 1s, 2s, 2p, 3s, and 3p derived orbitals occupied. The remaining dynamical electron correlation energy is obtained through second order perturbation theory (CASPT2). The basis set used in the calculations is of the atomic natural orbital (ANO-RCC) type contracted to  $9s8p7d5f3g$ . This basis set is relativistic and includes functions for correlating the 3s and 3p electrons [13]. The Douglas-Kroll Hamiltonian was used with Fock-type correction  $0.5 * \mathbf{g}_1$ , see [14]. The full counterpoise method was used to correct energies for the basis set superposition error (BSSE). Convergence to  $10^{-10}$ , in hartrees, was achieved, and numerical accuracy in computed binding energies was about  $10^{-8}$ .

For separations  $R \leq R_1^\lambda$ , where  $R_1^\lambda$  is the smallest separation of the *ab initio* data for the potential energy  $V_\lambda(R)$ , each curve was joined smoothly to the exponential form  $V_\lambda(R) = c_\lambda \exp(-b_\lambda R)$ , with the coefficients  $c_\lambda$  and  $b_\lambda$  determined by matching both the potential curve and its first derivative continuously at  $R_1^\lambda$ . At large values of  $R$ , the *ab initio* data were matched to the asymptotic form

$$V_\lambda(R) = -\frac{C_6}{R^6} + A_\lambda R^\nu e^{-\beta R},$$

where  $C_6$  is the van der Waals coefficient [15], and the

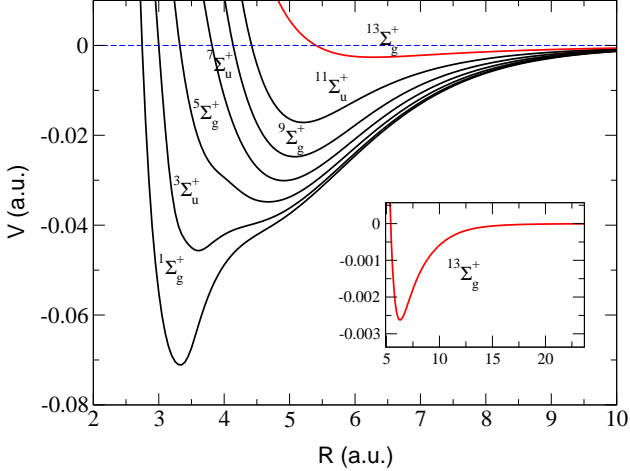


FIG. 1: Potential curves for the ground state manifold of  $\text{Cr}_2$  computed with the CASSCF/CASPT2 method. The maximally spin-stretched electronic state,  $^{13}\Sigma_g^+$ , is shown in red and in detail in the inset. This state supports 30 vibrational levels.

parameters of the exchange energy are determined according to Smirnov and Chibisov [16]:  $\nu = \frac{7}{2I} - 1$  and  $\beta = 2I$ , where  $I$  is the ionization energy of the atom ( $I = 0.248664314$  a.u. for Cr). The parameters  $A_\lambda$  were found by fitting the *ab initio* curves at separations where the exchange energy was still considerable (e.g.  $R$  between 10 and 14 a.u. for  $^{13}\Sigma_g^+$ ). The  $C_6$  coefficient was calculated using

$$C_6 = \frac{3}{2} \left( \frac{e^2 \hbar^2}{m} \right)^2 \frac{1}{|E_0|^3} \left\{ \sum_{i,j} \frac{f_{0i} f_{0j}}{v_i v_j (v_i + v_j)} + 2 \sum_i \frac{f_{0i} G(1 + v_i)}{v_i} + \int_0^\infty \frac{(df/d\epsilon) G(2 + \epsilon) d\epsilon}{(1 + \epsilon)} \right\}, \quad (1)$$

where contributions of bound-bound, bound-free, and free-free transitions are given by the first, second, and third term, respectively. This expression is derived from the London's [17] formula, assuming  $v_i = 1 - E_i/E_0$  and  $\epsilon = -E/E_0$ , where  $E_0$ ,  $E_i$ , and  $E$  are the ground, the  $i^{\text{th}}$  excited state and continuum energies, respectively,  $f_{0i}$  are the oscillator strengths pertaining to transitions to the ground states, and  $df/dE$  accounts for the continuous spectrum. The auxiliary function  $G(z)$  is given by

$$G(z) = \int_0^\infty \frac{(df/d\epsilon) d\epsilon}{(1 + \epsilon)(z + \epsilon)}. \quad (2)$$

Values of oscillator strengths and energy levels for discrete transitions were taken from the NIST Atomic Spectra Database [18] and Ref. [19]. The continuous oscillator strength,  $df/d\epsilon$ , was found using Verner's [20] analytic fits for partial photoionization cross sections. If we measure  $dE$  in atomic units then

$$\frac{df}{dE} = \frac{1}{2\pi^2 \alpha a_0^2} \sigma_{\text{ph}}, \quad (3)$$

where  $\alpha$  is the fine-structure constant,  $a_0$  is the Bohr radius, and  $\sigma_{\text{ph}}$  is the photoionization cross section. The dimensionless  $df/d\epsilon$  is obtained by multiplying Eq.(3) by  $|E_0|$  (also in a.u.).

We assess the quality of the semi-empirical computation of the van der Waals coefficient by satisfying two sum rules, namely, the zero-th and the inverse second moments,

$$S(0) = \sum_i f_{0i} = N$$

$$S(-2) = \alpha_0 = \frac{e^2 \hbar^2}{m |E_0|^2} \left\{ \sum_i \frac{f_{0i}}{v_i^2} + G(1) \right\}, \quad (4)$$

where  $N$  is the number of electrons (24 for Cr), and  $\alpha_0$  is the static polarizability. We obtained  $\sum_i f_{0i} = 22.3$  and  $\alpha_0 = 85.00$  a.u., in agreement with a recommended value  $82 \pm 20\%$  a.u. [21]). The resulting dispersion coefficient is expected to have an accuracy of about 7%,  $C_6 = 745 \pm 55$  a.u.

Using these potential curves, we computed the elastic  $\sigma_{\text{el.}}^\lambda$  cross section for the maximally spin-aligned molecular state, i. e. the  $^{13}\Sigma_g^+$  state. [Results for other molecular states and also inelastic and spin relaxation cross sections will be provided in a future publication.] The elastic cross section for the collision of two  $^{52}\text{Cr}$  atoms, composite bosons, expanded over the rotational quantum number,  $l$ , is [22]

$$\sigma_{\text{el.}}^\lambda(E) = \frac{8\pi}{k^2} \sum_{l \text{ even}} (2l + 1) \sin^2 \delta_l^\lambda, \quad (5)$$

where  $E = \hbar^2 k^2 / 2\mu$  is the kinetic energy of relative motion,  $\mu$  is the reduced mass, and  $\delta_l^\lambda(k)$  is the  $l$ -th scattering phase shift in electronic state  $\lambda$ . In the low-energy limit, the elastic cross section behaves as

$$\sigma_{\text{el.}}^\lambda(E) \xrightarrow{E \rightarrow 0} \frac{8\pi a_\lambda^2}{k^2 a_\lambda^2 + (1 - \frac{1}{2} r_\lambda a_\lambda k^2)^2}, \quad (6)$$

where scattering length  $a_\lambda$  is determined at the zero-energy  $s$ -wave limit,  $a_\lambda = -\lim_{k \rightarrow 0} \frac{1}{k} \tan \delta_0^\lambda(k)$ , while the effective range  $r_\lambda$  can be found by fitting the cross section, from an integral expression [22], or using quantum defect theory[23].

The cross section as a function of the collision energy is shown in Fig. 2 for three different  $^{13}\Sigma_g^+$  interaction potentials; each constructed by matching at large distances to the upper, lower, and mean values of  $C_6$ . Note that at collision energies larger than  $E \sim 10^{-6}$  a.u., aside from the shape resonance structure, the cross sections differ little in magnitude, but are dramatically different in the  $s$ -wave limit. We find the scattering length for the  $^{13}\Sigma_g^+$  state,  $a_{13}$ , to be large and negative (see Table I), indicating that evaporative cooling should be efficient, but that a Bose-Einstein condensate of  $^{52}\text{Cr}$  would not be stable for large number of atoms. This contrasts Ref. [5] in which the extracted value for the scattering

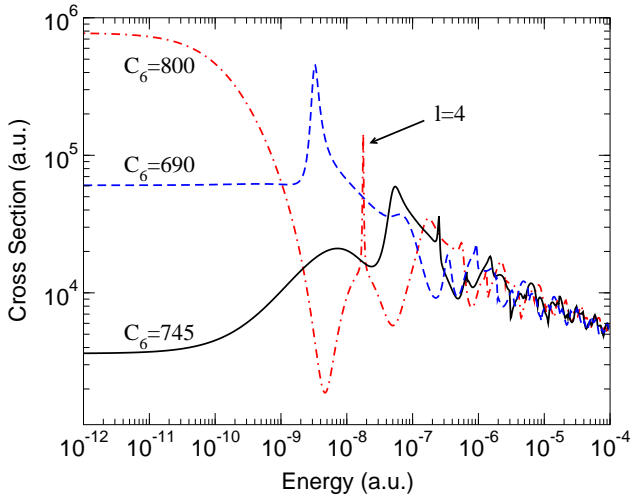


FIG. 2: Elastic cross sections for collision between two bosonic Cr atoms as a function of energy in the cold and ultracold regimes. The three curves are labeled by the value of the  $C_6$  coefficient used to construct the interaction potential in each case. See text for details. The influence of shape resonances is dramatic.

length, obtained from a fit to the experimental collision rate coefficient, Fig. 3, agrees in magnitude with our upper bound calculated value, but differs in the prediction of the sign (see also the discussion of the rates below). Our calculated effective range expansion coefficients also agree very closely with the results obtained using the quantum-defect method of Gao [23].

As the collision energy increases, the appearance of shape resonances can lead to enormously large cross sections. Although the details of the resonance structure, i. e. profile and energy position, depend on the details of the potentials, the overall effect on the collisional rate coefficient is only minimal at temperatures for which the shape resonances matter. This is portrayed in Fig. 3 for the ultracold and cold temperatures. The rate coefficients for the three different potentials are similar for temperatures higher than 100 mK. Our rate coefficients are larger than those measured by [7] by more than an order of magnitude. We do not yet understand the origin of this discrepancy- an attempt at modifying the potential in the long-range and in the short-range resulted in practically similar results. The shape and magnitude of the calculated rate coefficient for  $C_6 = 800$  a.u. agrees well in both magnitude and shape with the MOT experimental results, see Fig. 3 of Ref. [5]. The decline in the rate coefficient for  $T > 100 \mu\text{K}$ , as seen in our calculation, followed by a rise for  $T > 1 \text{ mK}$ , is due to the appearance of the  $l = 4$  shape resonance in Fig. 2. The experimental determination of the dip in the elastic rate could be used to infer a more accurate value of  $C_6$  and hence the scattering length as well.

In Fig. 4, we give the bound and shape resonance structure in the  $^{13}\Sigma_g^+$  potential energy curve with  $C_6 = 745$  a.u., as a function of the rotational angular momen-

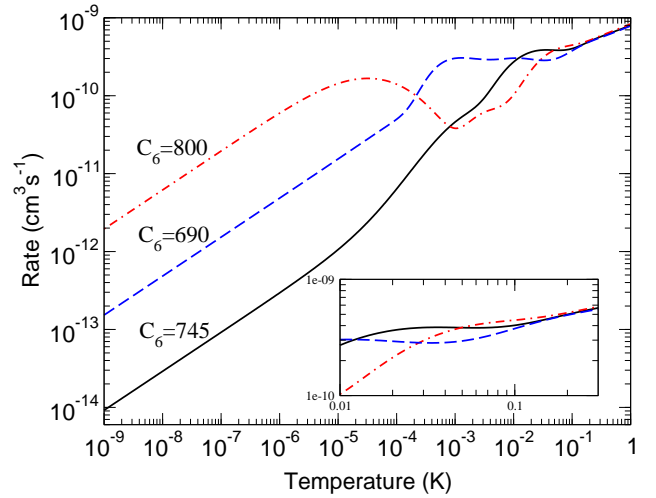


FIG. 3: The calculated collision rate coefficient as a function of temperature. At temperatures above 100 mK, the different calculated rates are practically the same. The plateau region is shown in the inset.

tum,  $l$ . Due to symmetry, only even values of  $l$  appear in the collision. There are 30 bound vibrational levels for the  $l = 0$  partial wave. The grouping of the levels in solid and dashed lines indicates the appearance of an additional shape resonance. Table II gives our calculated position and width for a number of rotational shape resonances. The narrowest resonance is for the  $l = 19$  partial wave with a lifetime of about two seconds. This resonance, however, is not populated in a bosonic collision.

A plateau in the observed elastic collision rate coefficient in the range  $10 \text{ mK} < T < 300 \text{ mK}$  exists [7, 8] and is reproduced in our calculation in Fig. 3. It appears that this plateau is produced by the confluence of many collisionally-excited shape resonances in this temperature range.

We have calculated *ab initio* interaction potentials for collision of two Cr atoms, and obtained the long-range van der Waals coefficient for the first time. Elastic collision cross section and rate coefficient for two maximally-stretched chromium atoms have been computed in the cold and ultracold regimes and compared with available experiments. The effect of partial-wave shape resonances is studied. The  $s$ -wave scattering length and effective range have been obtained in accord with experiment. The disagreement with the buffer-gas cooling rate coefficient results is not fully understood and the inelastic loss rate will be studied in the near future. The main loss rate mechanism is expected to be spin dipole interaction.

### Acknowledgments

The work of Z.P and R.C. was supported in part by the National Science Foundation grant PHY0140290 and University of Connecticut Research Foundation. The authors would like to thank J. Doyle and R. Krems for fruit-

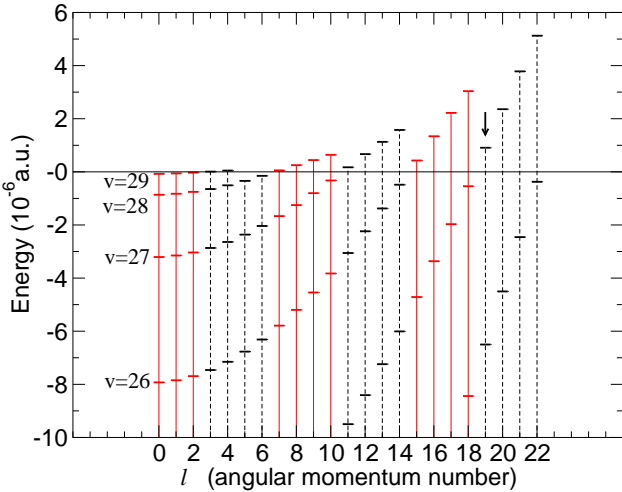


FIG. 4: The bound and shape resonance structure in the  $\text{Cr}_2$   $13\Sigma_g^+$  potential energy curve as a function of the rotational quantum number  $l$ .

ful discussions. This work was supported by the National

Science Foundation through a grant for the Institute for Theoretical Atomic Molecular and Optical Physics at Harvard University and Smithsonian Astrophysical Observatory. HRS is grateful to K. Andersson for access to numerical data for an earlier calculation of the potential curves and to P. O. Schmidt and R. deCarvalho for valuable correspondence. BOR thanks the Swedish Science Research Council (VR) for financial support.

C <sub>6</sub>	a <sub>13</sub>	r <sub>13</sub>
690	49	98
745	12	2600
800	-176	213

TABLE I: The calculated scattering length and effective range for different interaction potentials, all in atomic units.

---

[1] S. Chu, Rev. Mod. Phys. **70**, 685 (1998); C.N. Cohen-Tannoudji, *ibid*, 707; W.C. Phillips, *ibid*, 721.

[2] J. Weiner, V.S. Bagnato, S.C. Zilio, and P.S. Julienne, Rev. Mod. Phys. **71**, 1 (1999).

[3] See A. J. Leggett, Rev. Mod. Phys. **73**, 307 (2001), and references therein.

[4] C. C. Bradley, *et al.*, Phys. Rev. A **61**, 053407-1(2000).

[5] P. O. Schmidt *et al.*, arXiv:quant-ph/0303069 v2, 2003; P. O. Schmidt *et al.*, arXiv:quant-ph/0211032, Nov. 6 2002; P. O. Schmidt P.O. *et al.*, arXiv:quant-ph/0208129v1, Aug. 20 2002.

[6] Stuhler J. *et al.*, Phys. Rev. A **64**, 031405 (2001); S. Giovanazzi, A. Görlitz, and T. Pfau Phys. Rev. Lett. **89**, 130401(2002).

[7] J.M. Doyle *et al.*, Phys. Rev. A **65**, 021604 (2002); J. D. Weinstein *et al.*, Phys. Rev. A **57**, R3173(1998).

[8] Robert deCarvalho (private communication).

[9] L. Santos, G.V. Shlyapnikov, P. Zoller, and M. Lewenstein, *Bose-Einstein Condensation in Trapped Dipolar Gases*, Phys. Rev. Lett. **85**, 1791 (2000).

[10] M. Baranov *et al.*, arXiv:condmat/0201100 (2002)

[11] B. O. Roos in *Advances in Chemical physics, ab initio methods in quantum chemistry*, Ed. K. P. Lawley, John Wiley & Sons, Ltd., Chichester, 1987; B. O. Roos *et al.* in *Advances in chemical physics; new methods in computational quantum mechanics*, Ed. I. Prigogine and S. A. Rice, John-Wiley & Sons, Ltd., New-York, 1996.

[12] B. O. Roos, and K. Andersson, Chem. Phys. Letters **245**, 215 (1995); B. O. Roos, Collect. Czech. Chem. Commun. **68**, 265(2003); K. Andersson, Chem. Phys. Letters **237**, 212 (1995).

[13] The primitive basis set was: 21s15p10d6f4g. These basis sets are under construction for the entire periodic system (B. O. Roos, to be published).

[14] K. Andersson, Theor. Chim. Acta **91**, 31 (1995).

[15] Higher order dispersion coefficients, such as  $C_8$ ,  $C_{10}$ , etc., were not included in our analysis.

[16] B. M. Smirnov, and M. I. Chibisov, Soviet Physics JETP, **21** 624 (1965); E. L. Duman, and B. M. Smirnov, Optics and Spectroscopy, **XXIX** 229 (1970).

[17] H. Margenau, Phys. Rev., **56**, 1000 (1939).

[18] NIST Atomic Spectra Database : [http://physics.nist.gov/cgi-bin/AtData/main\\_asd](http://physics.nist.gov/cgi-bin/AtData/main_asd)

[19] D. A. Verner, P. D. Barthel, and D. Tytler, A&AS, **108**, 287 (1994).

[20] D. A. Verner, and D. G. Yakovlev, A&AS, **109**, 125 (1995).

[21] CRC Handbook of Chemistry and Physics, 83rd Edition, Section 10-163, Atomic and Molecular Polarizabilities, CRC Press, LLC, [www.crcpress.com](http://www.crcpress.com).

[22] N. F. Mott, and H. S. W. Massey, The Theory of Atomic Collisions. Third Edition. (1965)

[23] B. Gao, Phys. Rev. A P**58**, 4222(1998).

[24] Th. Dohrman *et al.*, J. Phys. B **29**, 4461 (1996).

[25] V. K. Dolmatov, J. Phys. B **26**, L393 (1993).

<i>l</i>	E (a.u)	$\Gamma$ (a.u)
3	8.04(-09)	5.82(-10)
4	4.82(-08)	2.87(-08)
7	5.38(-08)	2.03(-12)
8	2.52(-07)	1.60(-08)
9	4.44(-07)	1.04(-07)
10	6.41(-07)	2.81(-07)
11	1.72(-07)	1.10(-14)
12	6.66(-07)	2.27(-09)
13	1.13(-06)	6.11(-08)
14	1.58(-06)	2.42(-07)
15	4.27(-07)	6.32(-17)
16	1.34(-06)	1.11(-10)
17	2.22(-06)	1.82(-08)
18	3.04(-06)	1.59(-07)
19	9.07(-07)	$\ll 1$ (-17)
20	2.36(-06)	4.08(-12)
21	3.78(-06)	2.70(-09)
22	5.12(-06)	7.10(-08)

TABLE II: The rotational shape resonance parameters, position and width, in the  ${}^{13}\Sigma_g^+$  potential. Note that only even partial waves contribute to the scattering of spin polarized bosons (odd partial waves are included for completeness).